Arch. Metall. Mater. **70** (2025), 2, 973-981

DOI: https://doi.org/10.24425/amm.2025.153502

U.K. TARAI[1], S. DWIBEDI[2], D.R. BISWAL[1], A.R. BISWAL[1],
MADHAB BEHERA[1], SUYOG JHAVAR[3*]

INFLUENCE OF PROCESS PARAMETERS ON THE MICROSTRUCTURAL AND MECHANICAL CHARACTERISTICS OF TLP BONDED IN718

Inconel 718 (IN718) superalloy is joined through transient liquid phase bonding using a interlayer material (BNi-2). This study explores the role of process parameters in joining IN718 with the TLP bonding process is explored. Microstructure evolution and mechanical performance of the bond are investigated using scanning electron microscopy, tensile test, and micro-hardness test. The bond metallurgy showed three distinct zones: the base material zone, the diffusion-affected zone containing a large number of boride precipitates, and the isothermal solidification zone. Further investigation reveals that the ISZ contains a few brittle intermetallic particles, which reduce the mechanical properties of the bond. The results demonstrates that higher bonding temperature, time, optimal interlayer thickness, and pressure enhance the mechanical and microstructural properties of the bond. The bond formed at 1423 K bonding temperature, 1.5 h holding time, 80 μm interlayer thickness, and 12.5 kg load demonstrates the highest strength of 625 MPa.

Keywords: IN718; TLP bonding; Interlayer; Inconel 718; Diffusion

1. Introduction

Gas turbine engines are widely utilized in both aircraft and land-based power generators. As these engines are exposed to severe working environments at elevated temperatures, corrosion resistance, tensile and creep strength are essential to endure the imposed loads. To address these requirements, nickel-based superalloys are predominantly used as the raw material for fabricating gas turbine components. The precipitates (γ' and γ''), along with carbides in most Ni-based superalloys, confer outstanding strength and corrosion resistance at raised temperatures [1-3]. In contrast to other Ni-based superalloys, IN718 exhibits superior resistance to cracking (strain age) while joining or post-weld heat treatment (PWHT) [4]. For the past 60 years, this superalloy has been a fundamental material in manufacturing many gas turbine components [5]. IN718 is used in high-temperature applications, such as turbine disks, blades, space shuttle rocket engines, and compressors [6-8]. Previously, various casting processes produced gas engine parts as single components. However, single-cast components typically exhibit inferior properties and a more inhomogeneous microstructure [9]. Therefore, it is essential to produce engine components in smaller segments and then joined using suitable bonding techniques.

Furthermore, as aero-engine components are subjected to high creep and fatigue loads in extreme working environments, degradation of these components is often observed. Economic factors make it more cost-effective to refurbish and repair parts instead of replacing expensive, damaged components. Over the years, various methods for joining turbine components have been developed, including electron beam welding (EBW), gas tungsten arc welding (GTAW), plasma arc welding (PAW), and laser beam welding (LBW) [10], as well as high-temperature brazing [11] and solid-state diffusion bonding [12]. However, problems such as micro-fissuring, compositional loss, and brittle intermetallic are observed during welding [13,14]. Micro-fissuring's are fine cracks, typically two grains long, that develop in the heat-affected zone (HAZ) [15,16]. Brazing often results in the formation of brittle eutectic phases in the joint area, which reduces the mechanical strength of the joint. Consequently, this process is generally not recommended for joining or repairing IN718 components. Solid-state diffusion bonding often requires high pressure, which can distort the thin section components [12].

[1] DRIEMS UNIVERSITY, DEPARTMENT OF MECHANICAL ENGINEERING, CUTTACK 754022, INDIA
[2] DEPARTMENT OF MECHANICAL ENGINEERING, INDIAN INSTITUTE OF TECHNOLOGY GUWAHATI, ASSAM 781039, INDIA
[3] VIT-AP UNIVERSITY, SCHOOL OF MECHANICAL ENGINEERING, AMARAVATI, ANDHRA PRADESH 522237, INDIA

* Corresponding author: suyog.jhavar@vitap.ac.in

To address these issues, researchers introduced the transient liquid phase (TLP) bonding process [17,18]. Utilizing the benefits of brazing and solid-state diffusion bonding, TLP technique was developed to join hard-to-weld superalloys. In the TLP bonding, an interlayer is positioned between the base material (BM), and the setup is then heated above the melting temperature of the interlayer and maintained for an adequate time periods. After the interlayer melts, the BM dissolves, causing the liquid region to expand. Upon holding at higher temperatures, inter-diffusion of atoms occurs through the interface, establishing equilibrium in solute concentration at the interface. As a result, isothermal solidification (IS) begins. As holding continues, the liquid's width decreases due to IS, causing the solid-liquid interface to move toward the center of the joint. If the assembly is held long enough, the liquid undergoes complete IS. However, if the holding time is inadequate, the residual liquid at the joint can transform into eutectic-type brittle phases, potentially diminishing the bond's mechanical properties [19]. These eutectics can be reduced through proper homogenization techniques [20].

Numerous studies have been conducted on joining IN718 using TLP bonding [21,22]. Previous studies have shown that the amount of eutectic formation in the bond area is highly influenced by process parameters (bonding temperature (T_{bond}), holding time (t_{hold}), pressure (P_{bond}), and interlayer thickness (T_w)) and metallurgical factors [23]. Kim et al. [24] studied the impact of t_{bond} and T_{bond} on the metallurgy aspects and observed that increasing both t_{bond} and T_{bond} improved the strength of the TLP-bond. However, beyond a specific temperature, the isothermal rate decreases. Saha and Khan [25] investigated the influence of input bonding parameters on the TLP bonding of superalloys (oxide dispersion-strengthened). They reported that applying bonding pressure decreased the width of the joint and the number of inclusions near the interface. Cho et al. [26] studied the influence of interlayer (thickness) and alloying on the microstructure development, and mechanical reliability of TLP bonding. The research found that a thicker interlayer facilitated proper bonding, whereas a thinner interlayer led to defective bonds.

It is observed that considerable research has been conducted on the effects of process parameters, wherein most studies have examined these parameters individually. However, the combined impact of process parameters has not been reported. Therefore, the current research investigates the combined effects of T_{bond}, t_{hold}, and T_w on the isothermal solidification time and bond properties of IN718.

2. Experimental Procedures

The IN718 is procured from a commercial supplier as 10 mm diameter rods. Cylinders with a nominal height of 72 mm are machined from these rods using wire-cut EDM. The faying surfaces of each cylinder were ground flat using silicon carbide polishing discs with grit sizes of 220-1000, in that order, to achieve a uniform and consistent surface roughness. Following the grinding process, each sample is cleaned ultrasonically in acetone for 10 minutes to remove any remaining impurities or debris, such as SiC particles, ensuring a clean faying surface. In this research, the interlayer material used for TLP bonding experiments is a commercially available amorphous BNi-2 foil with a thickness of 40 μm and a width of 10 mm. The elemental composition of the IN718 superalloy and the interlayer material used in the present investigation is listed elsewhere [27]. Nine experiments are conducted by varying the process parameters using an in-house designed set-up, as shown in Fig. 1. The utilized process parameters are detailed in TABLE 1.

For microstructural examination of the TLP bond, samples were cut perpendicular to the bond-line using wire-cut electro discharge machining. Then, the samples are polished to a mirror finish using the standard microstructural procedure. The polished samples were etched by immersing them for 120 s in a freshly prepared etchant consisting of 15 ml glycerol, 10 ml HCl, and 5 ml HNO_3. Subsequently, the microstructure of the sample is investigated using a field emission scanning electronic microscope (FESEM) coupled with an energy dispersive X-ray spectroscopy (EDS) system and optical microscope. The EDS analysis is carried out at an acceleration voltage of 20 kV using a secondary electron detector. Round tensile samples are fabricated (ASTM-E8M) using a lathe machine, with a gauge length of 24 mm and a diameter of 6 mm. Tensile test is conducted on a universal testing machine at 0.5 mm/min crosshead speed. The hardness variation in various regions of the bond is measured using a micro-hardness tester with 300 gf force and 15 sec dwell time.

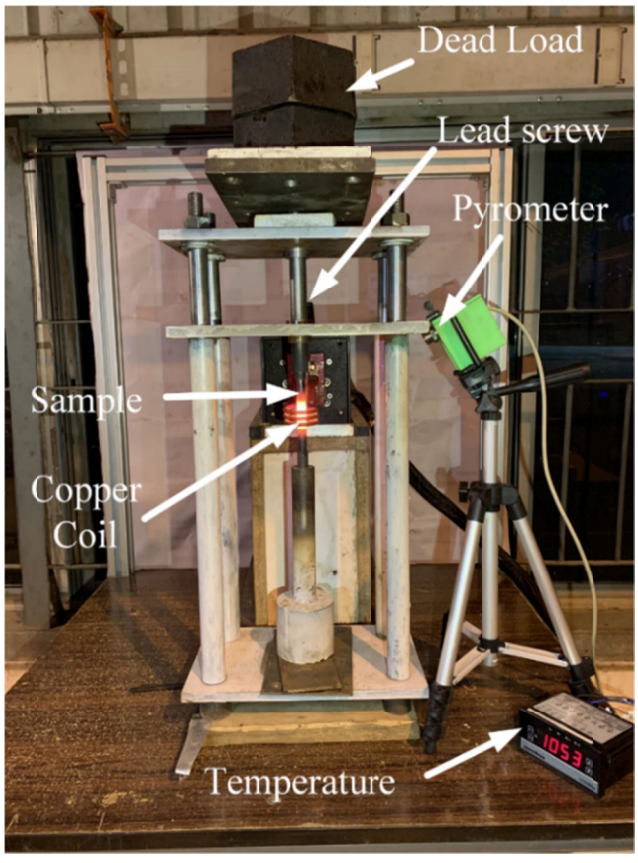

Fig. 1. Developed experimental set-up for TLP bonding

TABLE 1

Process parameters utilized for TLP bonding

Case	Temperature, K	Time, h	Interlayer thickness, µm	Load, Kg
S.1	1323	1	80	12.5
S.2		1.5	120	15.7
S.3		2	160	19.6
S.4	1373	1	120	19.6
S.5		1.5	160	12.5
S.6		2	80	15.7
S.7	1423	1	160	15.7
S.8		1.5	80	19.6
S.9		2	120	12.5

3. Results and discussion

3.1. Microstructural evaluation

The optical micrograph of the as-received IN718 and the BMZ is depicted in Fig. 2(a-b). The microstructures display an austenite γ-matrix with finely dispersed metallic carbide precipitates. According to EDS analysis (Fig. 2(c)), the larger, irregularly shaped precipitates are carbide particles, predominantly Nb carbides. The grain size (GS) of the samples is measured according to ASTM-E112 standards using the line intercept method. The GS of the BM and the bonded coupons is identified as 20 and 60 µm, respectively. The GS increases during TLP bonding, which can be attributed to the exposure of samples to high temperatures during the IS stage, resulting in recrystallization and grain growth.

The TLP-bonded samples for samples S.2, S.6, and S.8 are shown in Fig. 3(a-c). During the TLP joining of Inconel alloys, different zones are identified: (a) IS-Zone (isothermal solidified zone), (b) AS-Zone (athermal solidified zone), and (c) DA-Zone (diffusion affected zone). During the bonding of IN718 using the interlayer (BNi-2), elements from the liquid BNi-2 interlayer and the IN718 BM undergo inter-diffusion. The melting point depressant (MPD) elements (B and Si) diffuse from the liquid interlayer into the BM, while elements like Ti, Nb, Al, Mo, and Cr from the BM diffuse into the liquid interlayer [21]. The interdiffusion of elements is confirmed through the EDS and EDS line scan results, presented in the subsequent sections. This inter-diffusion alters the MPD composition at the interface, moving it away from the eutectic composition and raising the melting point of the interlayer. As a result, a new solid interface forms, and the width of the liquid zone gradually decreases until it disappears entirely. The solidified area created

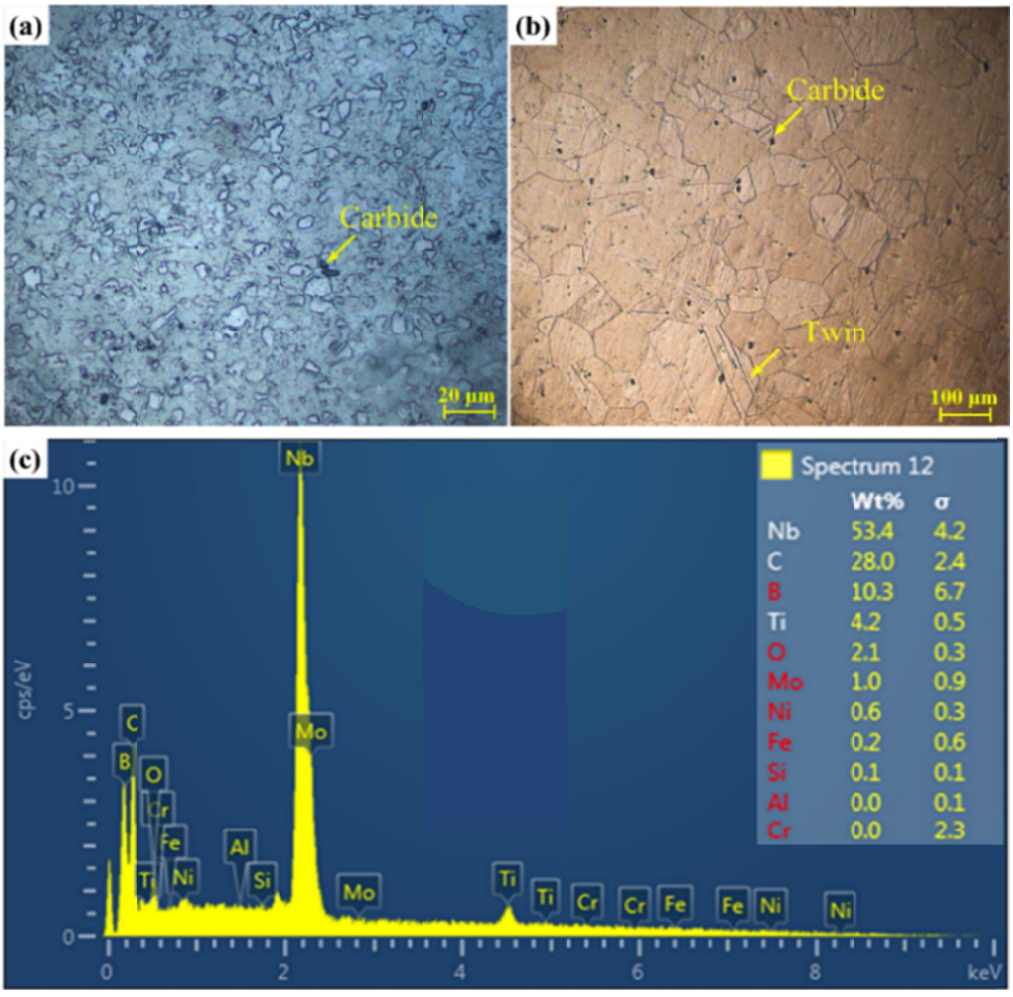

Fig. 2. FESEM microstructure of (a) as-received IN718 and (b) BMZ, and (c) elemental analysis of carbide precipitate

during IS is known as the IS-Zone. If the liquid does not fully solidify during the IS process, the remaining liquid solidifies athermally. Upon cooling, this leads to the formation of eutectic compounds at the bond centreline, referred to as the AS-Zone. In TLP bonding, the IS-Zone width becomes smaller than the initial interlayer thickness due to the inter-diffusion of elements and the applied pressure. In sample S.1, the initial interlayer thickness is 80 µm, but after IS, the IS-Zone width decreased to 45 µm. This can be attributed to the reduction in the liquid width caused by inter-diffusion during the heating and melting phase [28]. When the temperature is increased, the IS-Zone width also increases. For experiments S.6 and S.8, the IS-Zone widths are 57 µm and 71 µm, respectively, even though the initial interlayer thickness is 80 µm in both cases. This increase in IS-Zone width at higher temperatures is likely due to more dissolution and widening of the BM. The elements that diffused from the liquid interlayer into the BM react with the BM elements to form secondary particles present in the DA-Zone. Beyond the DA-Zone, the unaffected BM-Zone is observed, where the chemical composition remains relatively unchanged, although grain growth may occur.

The DA-Zone of the TLP-bonded S.2 sample is shown in Fig. 4(a), which highlights the precipitates (metallic) formed in the DA-Zone. These precipitates have various shapes, including needle-like, coarse irregular shapes, and fine blocky forms. The elemental analysis results are depicted in Fig. 4(b-d). δ-phases (in IN718) are typically found at the GB (grain boundary), resulting in higher Nb content at the boundaries compared to the grains. Additionally, GBs have a higher affinity for diffusion, leading to more boride formation in those areas. Although boron is not detected in the EDS analysis, previous studies on TLP bonding of Inconel superalloy using BNi-2 interlayer material have reported that these precipitates are borides [19,22,23]. These precipitates are rich in Nb, Cr, and Mo. The analysis confirms the precipitates as borides (Nb–Mo–Cr type). However, published research suggests M_3B_2 (fine blocky), M_6B (coarse blocky), and M_4B_3 (chain-like borides) type borides [29-31]. Fig. 4(e) presents the area mapping of the DA-Zone in the TLP-bonded joint corresponding to sample S.2, providing critical insights into the microstructural evolution and precipitate distribution, particularly of Nb, Mo, and Cr borides. The mapping clearly illustrates the spatial distribution and morphology of the precipitates, identifying regions where Nb, Mo, and Cr have interacted with the boron-rich liquid phase to form distinct boride compounds. Although the distribution of B is uniform, particularly in regions with a substantial rise in the concentrations of Nb, Mo, and Cr, the past studies reveal that the precipitates are rich in B [21,27]. The results reaffirm that the borides are rich in Nb, Mo, and Cr. Fig. 4(f) provides the magnified view of the IS-Zone, showing the presence of black and gray precipitates. The elemental analysis for the areas D, E, F, and G are summarized in Fig. 4(g), wherein Nb, Mo, Al, Ti, and Si are present in the ISZ. The presence of these elements in the IS-Zone suggests they diffused from the BM into the bond zone during the melting, dissolution, and IS process [19]. The EDS results also reveal that Al-rich precipitates are formed in the AS-zone. The precipitate present inside the rectangle D marked in the Fig. 4 (f) is an Al-rich Si. The EDS analysis result of the precipitate present inside E and G are Ni,

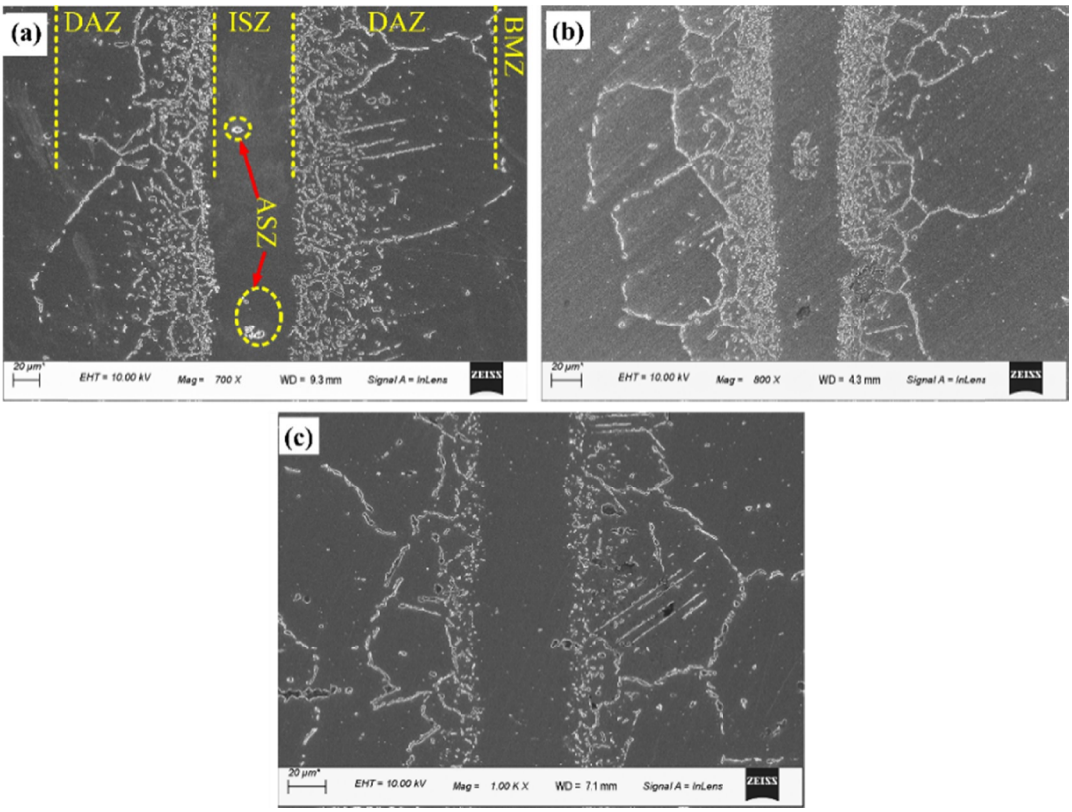

Fig. 3. Microstructure of the TLP bonded sample corresponding to expt. no. (a) S.2, (b) S.6 and (c) S.8

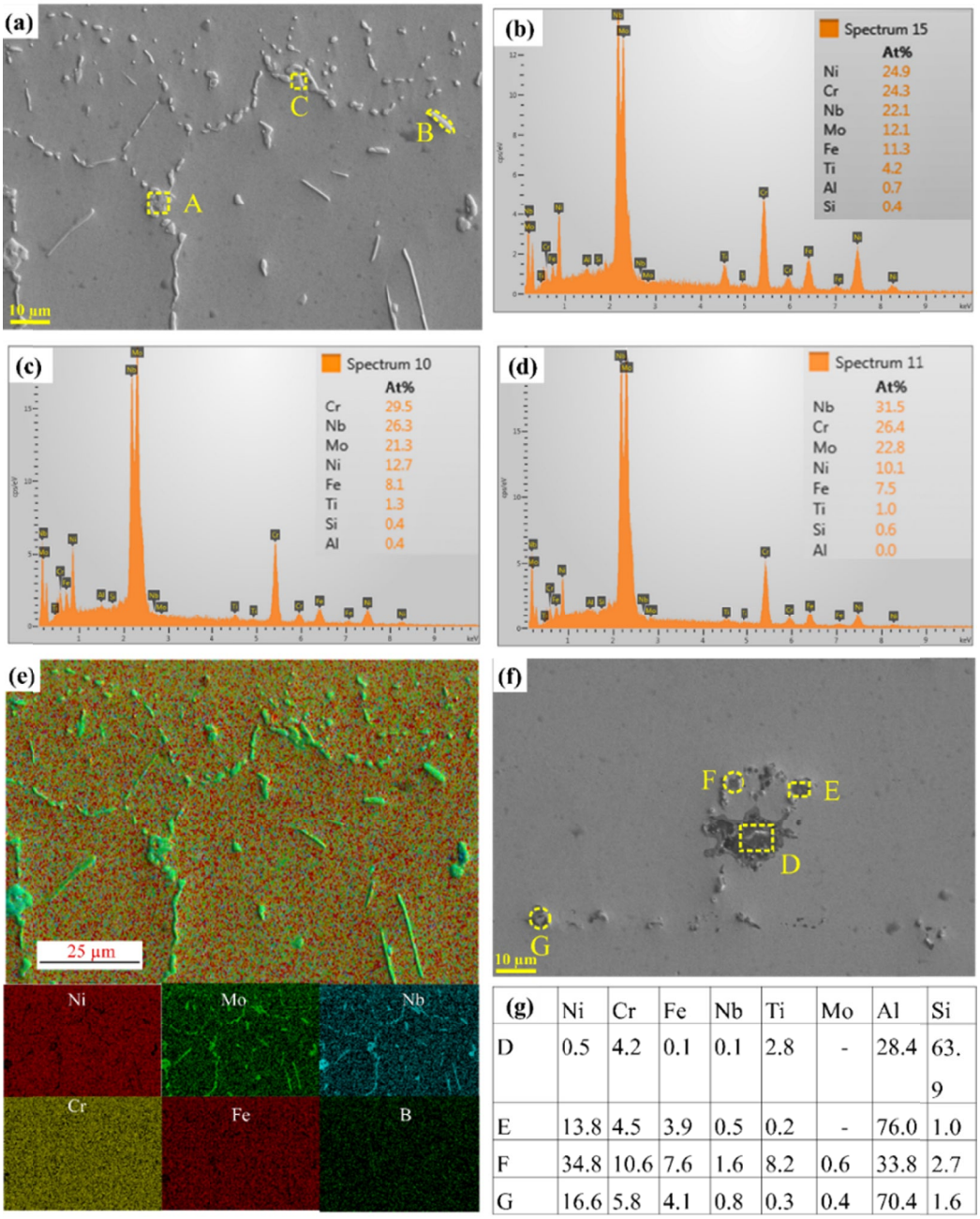

(g)	Ni	Cr	Fe	Nb	Ti	Mo	Al	Si
D	0.5	4.2	0.1	0.1	2.8	-	28.4	63.9
E	13.8	4.5	3.9	0.5	0.2	-	76.0	1.0
F	34.8	10.6	7.6	1.6	8.2	0.6	33.8	2.7
G	16.6	5.8	4.1	0.8	0.3	0.4	70.4	1.6

Fig. 4. (a) Magnified view of the DA-Zone (b-d) EDS result corresponding to precipitate present in areas highlighted in (a), (e) area mapping of the DA-Zone, (f) close-up view of the IS-Zone for sample S.2, and (g) chemical composition of precipitates highlighted in (f)

Al, Fe, Cr, and Si rich compound contains some trace of Nb, Ti and Mo. The EDS analysis results of the precipitate present inside the rectangle F indicate that the precipitate is rich in Ni, Al, Ti, Fe, Cr, and Si. These precipitates were formed due to the interdiffusion of elements between the BM and the interlayer. The size and amount of these precipitates decreases when the T_{bond} is increased and a more uniform microstructure is achieved when the bond is held at a higher temperature and for a longer T_{bond}, compared to bonds made with lower temperatures and shorter T_{bond}.

Fig. 5(a) reveals the precipitates as Al, Ti, and Si-rich compounds. The precipitates are silicides of Ti and Al (IS-Zone due to incomplete IS). The elemental distribution (Fig. 5(b)) remains relatively consistent across all zones, except where the line scan intersects with precipitates. At these intersection points, there are noticeable changes in the elemental composition, marked by increase/decrease. In the DA-Zone, where the scan line crosses precipitates, there is a significant rise in the levels of Nb, Mo, Cr, and B, while the Fe and Ni content decreases. These fluctuations in the DA-Zone are attributed to the presence of Nb, Cr, and Mo-rich precipitates. At the center of the IS-Zone, a noticeable increase in Ti, Al, and Si peaks is observed, indicating the presence of Al, Ti, and Si-rich compounds. At the start, there is no Al or Ti (interlayer), but in the course IS, these elements diffused to the liquid interlayer, forming Al, Ti, and Si-rich compounds in the IS-Zone.

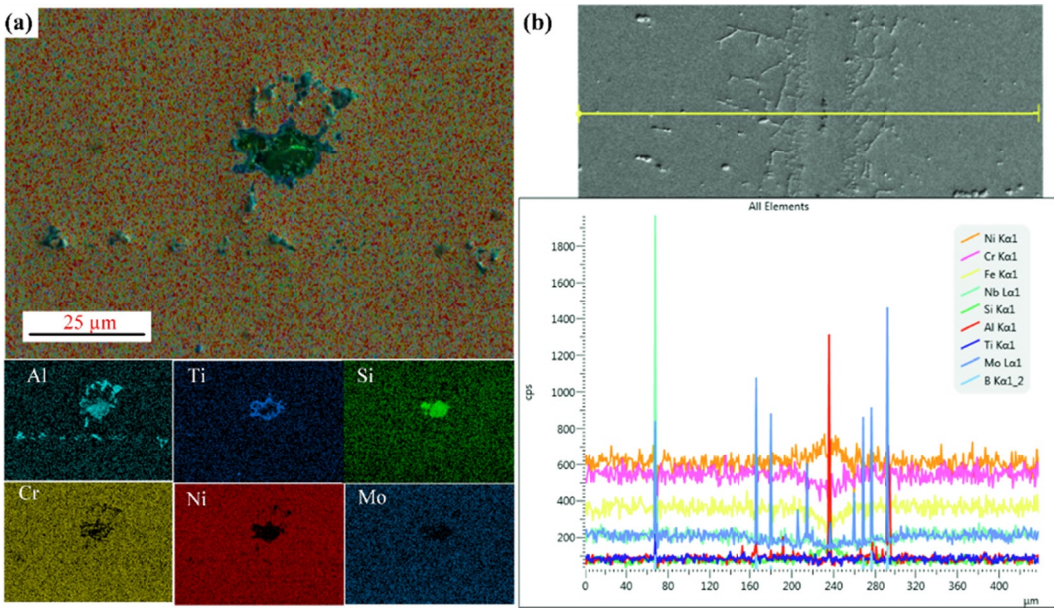

Fig. 5. (a) Area elemental mapping of the IS-Zone of sample S.2 and (b) line scan analysis of the TLP-bonded sample corresponding to sample S.2

3.3. Mechanical properties

Fig. 6(a-c) shows the tensile properties of the bonded samples. The results indicate that the maximum bond strength (625 MPa), with 85 % joint efficiency of the BM [32], is achieved at 1423 K T_{bond}, with a 1.5 h t_{hold}, 80 µm interlayer thickness, and a 19.6 kg load. The joint properties depend on the amount of solution-strengthening elements (Mo, Ti, Al, and Nb) diffused from the IN718 alloy into the bond zone and the amount of eutectic phases formed due to incomplete IS [21,22]. As TLP-bonding proceeds, the elements diffuse from the BM into the liquid interlayer. If the process does not last long enough, incomplete IS occurs, leading to the formation of eutectics in the bond zone, which weakens the bond [33]. The reduced UTS is due to this

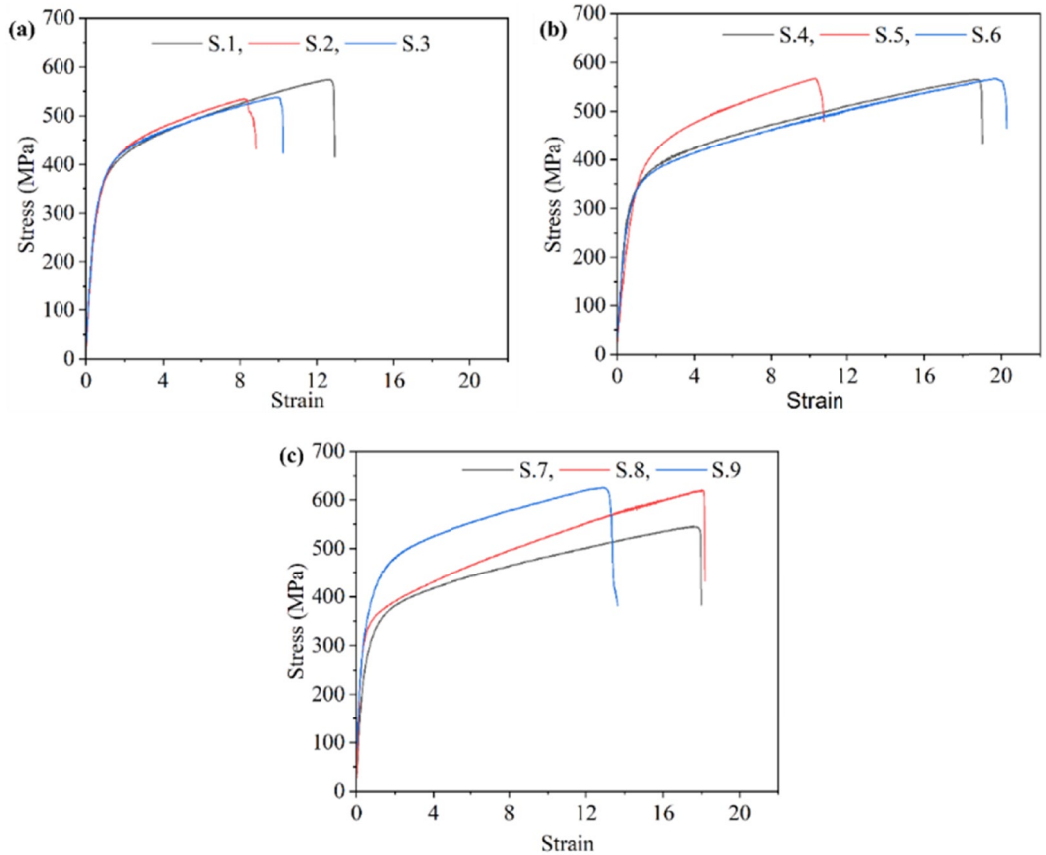

Fig. 6. Stress-strain curve of the samples fabricated at (a) 1323 K, (b) 1373 K and (c) 1423 K

incomplete solidification. It is also observed that bond strength increases at higher T_{bond}. At these higher temperatures, more interdiffusion occurs between the BM and the liquid interlayer, increasing the amount of solid solution elements in the IS-Zone while reducing the formation of eutectics [18,24]. This results in a stronger bond. Additionally, bond strength depends significantly on the IS time. Longer t_{bond} allow for more extensive diffusion of elements, resulting in a more uniform microstructure and, consequently, a stronger joint.

The ductility of the bonded sample is lower than that of the BM due to brittle secondary phases in the IS-Zone, which breaks during plastic deformation, reducing the bond zone's ductility [34]. However, samples at higher T_{bond} and longer t_{bond} show improved tensile strength and ductility. At higher T_{bond}, the rate of IS increases, which results in more Nb, Cr, Mo, Al, and Ti being incorporated into the IS-Zone. If the t_{bond} is extended at a constant temperature, more alloying elements diffuse from the BM into the ISZ. This leads to an increase in the bond strength. At longer t_{bond} and higher temperatures, more interdiffusion occurs, reducing the amount of unwanted phases in the IS-Zone. Although higher T_{bond} and longer t_{bond} improve strength, the failure zone remains in the IS-Zone due to brittle eutectic phases and lower amounts of solid solution-strengthening elements. The fractured specimens of the fabricated samples for the experiment numbers S.2, S.6, and S.8 are illustrated in Fig. 7(a-c). The fracture images comprise fine dimples and cleavage facets in some localized regions. The presence of centerline brittle precipitates in the AS-Zone serve as sites for easy crack initiation. During tensile loading, these particles provide a path that facilitates crack propagation and leads to eventual brittle failure. However, the IS-Zone consists of a γ-matrix, which absorbs a significant amount of plastic deformation, resulting in ductile failure. The combination of dimples, voids, and cleavage features suggests that the TLP-bonded IN718 joints experienced a mixed-mode failure. The dimples imply that the failure occurred through the initiation → growth → coalescence of micro-voids.

Fig. 8(a-c) reveals that the DA-Zone has the highest hardness among all zones in the TLP-bonded samples, while the ISZ has a hardness nearly equal to that of the BM-Zone. The hardness of the IS-Zone depends on two main aspects: (i) the amount of secondary phases and (ii) the concentration of solution-strengthening elements. The IS-Zone hardness in samples made at 1323 K is modestly higher than that of the BM-Zone, which is due to secondary (hard and brittle) precipitates in the IS-Zone at lower T_{bond}. If the t_{bond} is insufficient, the residual liquid stays in the IS-Zone, increasing its hardness. However, for bonds made at higher temperatures, the IS-Zone hardness is lower than that of the BM. Because at higher temperatures, the increased diffusion rate reduces the amount of residual liquid and secondary phase, while increasing the solution-strengthening elements. If the t_{bond} is too short, there will be fewer of these strengthening phases in the IS-Zone relative to the BM-Zone, leading to lower hardness at higher T_{bond}. The DA-Zone exhibits greater hardness than the BM-Zone and IS-Zone due to intermetallic precipitates (Mo–Nb rich boride). The BM-Zone hardness remains largely unaffected by the MPD elements. However, the BM-Zone hardness at higher T_{bond} is marginally less than at lower temperatures, due to grain growth occurring at higher temperatures.

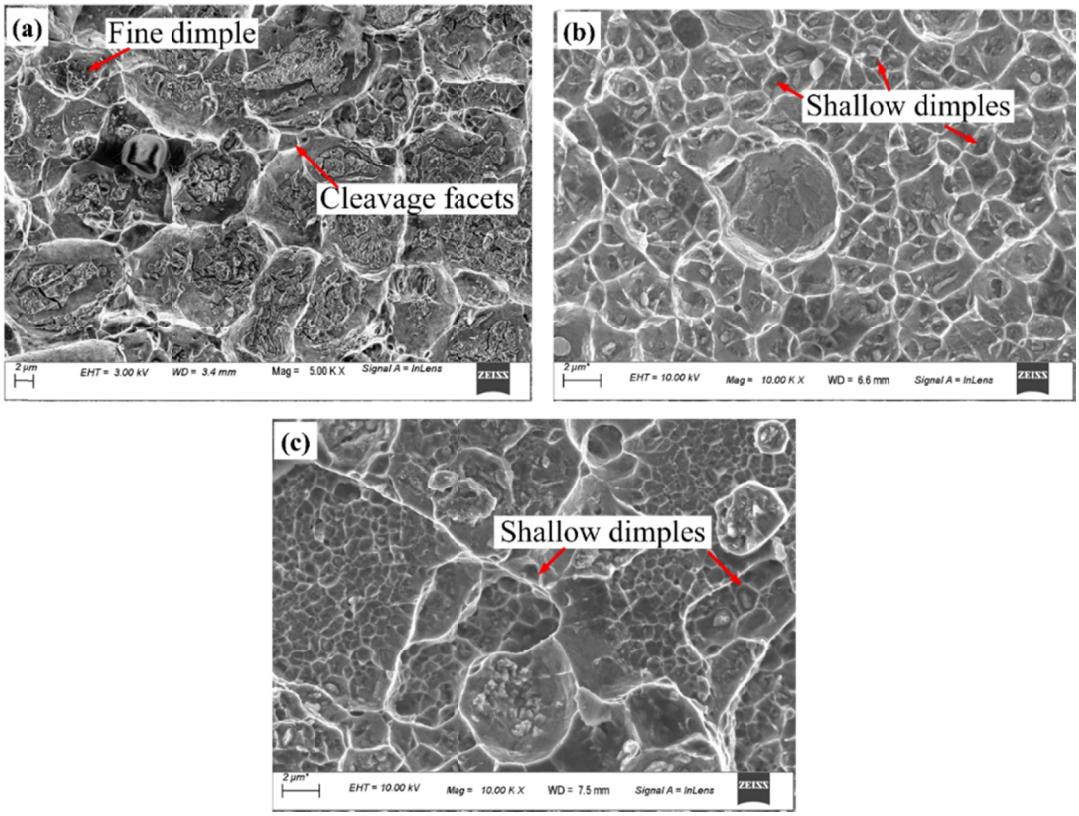

Fig. 7. Depicts fracture region of the samples (a) S.2, (b) S.6, and (c) S.8

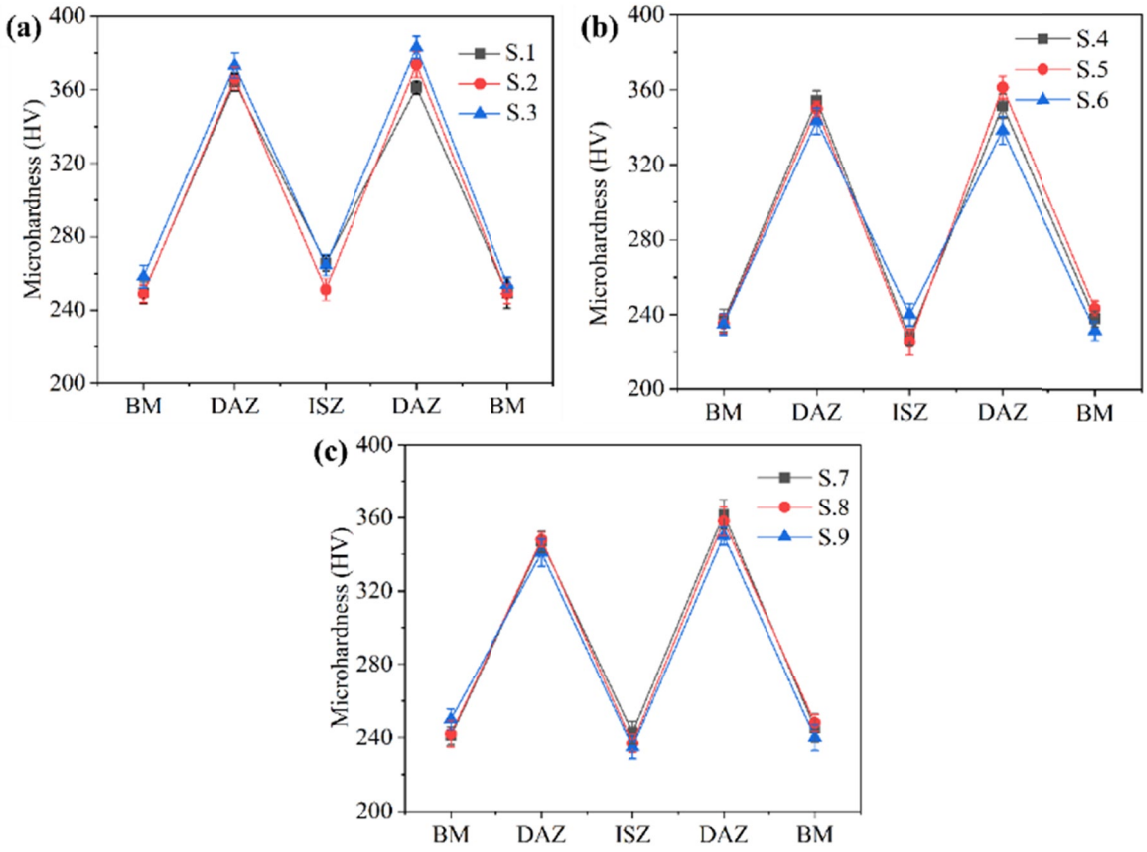

Fig. 8. Micro-hardness plot for the TLP-bonded sample fabricated at (a) 1323 K, (b) 1373 K, and (c) 1423 K

4. Conclusion

In the present work, a detailed experimental investigation is accomplished to evaluate the effect of input variables on the bond properties of the TLP-bonded IN718. The major highlights include: (a) the occurrence of Al-Ti-Si rich compounds in the athermal solidified zone reduces the strength of the bond, as these are the sites of easy crack initiations, (b) TLP-bonded joint formed at a 1423 K bonding temperature, with a 1.5 h holding time, 80 μm interlayer thickness, and a 12.5 kg load, achieved a maximum strength of 625 MPa, and (c) increasing bonding time and temperature increases the diffusion rate of elements in the bond zone, which enhances the tensile strength of the bond.

REFERENCES

[1] P.C. Gasson, The Superalloys: Fundamentals and Applications RC Reed Cambridge University Press. The Edinburgh Building, Shaftesbury Road, Cambridge, CB2 2RU, UK, 2006. 372 pp. Illustrated.\pounds 80. ISBN 0-521-85904-2, Aeronaut. J. **112**, 291-291 (2008).

[2] P.S. Gowthaman, S. Jeyakumar, A review on machining of high temperature aeronautics super-alloys using WEDM. Mater. Today Proc. **18**, 4782-4791 (2019).

[3] D.G. Backman, J.C. Williams, Advanced Materials for Aircraft Engine Applications. Science **255**, 1082-1087 (1992).

[4] X. Cao, B. Rivaux, M. Jahazi, J. Cuddy, A. Birur, Effect of pre-and post-weld heat treatment on metallurgical and tensile properties of Inconel 718 alloy butt joints welded using 4 kW Nd: YAG laser. J. Mater. Sci. **44**, 4557-4571 (2009).

[5] S. Miller, Advanced materials mean advanced engines. Interdiscip. Sci. Rev. **21**, 117-129 (1996).

[6] O.E. Oshobe, Fiber laser welding of nickel-based superalloy Inconel 718. University of Manitoba (Canada), (2012).

[7] S.R. Singh, R.G. Mote, S.K. Mishra, The effect of microstructures and precipitates (γ', γ″, δ) on machinability of Inconel-718 nickel-based superalloy in turning process. J. Manuf. Process. **82**, 374-389 (2022).

[8] S. Dwibedi, S. Bag, Critical assessment on the influence of process parameters in micro-plasma arc welding process: a review. Weld. Int. **38**, 583-617 (2024).

[9] S. Ozer, G.M. Bilgin, K. Davut, Z. Esen, A.F. Dericioglu, Effect of post fabrication aging treatment on the microstructure, crystallographic texture and elevated temperature mechanical properties of IN718 alloy fabricated by selective laser melting. J. Mater. Process. Technol. **306**, 117622 (2022).

[10] R. Kataria, R.P. Singh, P. Sharma, R.K. Phanden, Welding of super alloys: a review. Mater. Today Proc. **38**, 265-268 (2021).

[11] X. Huang, W. Miglietti, Wide gap braze repair of gas turbine blades and vanes – a review. (2012).

[12] D.P. Kumar, S. Kumaran, Mechanical and corrosion behaviour of Inconel 718 processed through SPS diffusion bonding and double aging treatment. Mater. Today Proc. **27**, 2582-2585 (2020).

[13] R.G. Thompson, Microfissuring of Alloy 718 in the Weld Heat-Affected Zone. JOM **40**, 44-48 (1988).

[14] M. Prager, C.S. Shira, Welding of precipitation-hardening nickel-base alloys(Welding precipitation hardenable Ni base alloys noting heat treatment, microfissuring, strain age cracking and other intricacies). Weld. Res. Counc. Bull. (1968).

[15] J. Zalawadia, K.K. Lamba, Experimental Investigation on Metallurgy of High Vacuum Electron Beam Welded Ni Base Alloy Inconel 718. Indian Weld. J. **50** (2017).

[17] D.H. Jung, A. Sharma, M. Mayer, J.P. Jung, A Review on Recent Advances in Transient Liquid Phase (TLP) Bonding for Thermoelectric Power Module. Rev. Adv. Mater. Sci. **53**, 147-160 (2018).

[18] B.K. Lee, W.Y. Song, D.U. Kim, I.S. Woo, C.Y. Kang, Effect of bonding temperatures on the transient liquid phase bonding of a directionally solidified Ni-based superalloy. GTD-111, Met. Mater. Int. **13**, 59-65 (2007).

[19] M. Pouranvari, A. Ekrami, A.H. Kokabi, Diffusion brazing of cast INCONEL 718 superalloy utilising standard heat treatment cycle. Mater. Sci. Technol. **30**, 109-115 (2014).

[20] W. Li, X. Li, Y. Liu, Z. Wang, C. Liu, H. Li, Homogenization stage during TLP bonding of RAFM steel with a Fe–Si–B interlayer: microstructure evolution and mechanical properties. Mater. Sci. Eng. A **780**, 139205 (2020).

[21] M. Pouranvari, A. Ekrami, A.H. Kokabi, Transient liquid phase bonding of wrought IN718 nickel based superalloy using standard heat treatment cycles: Microstructure and mechanical properties. Mater. Des. **50**, 694-701 (2013).

[22] G. Yan, A. Bhowmik, B. Nagarajan, X. Song, S.C. Tan, M.J. Tan, The bonding time effects on the transient liquid phase bonding of Inconel 718 using nickel-based sintered brazing preform. Appl. Surf. Sci. **495**, 143465 (2019).

[23] A.T. Egbewande, C. Chukwukaeme, O.A. Ojo, Joining of superalloy Inconel 600 by diffusion induced isothermal solidification of a liquated insert metal. Mater. Charact. **59**, 1051-1058 (2008).

[24] J.K. Kim, H.J. Park, D.N. Shim, D.J. Kim, Effect of bonding parameters on microstructural characteristics during TLP bonding of directionally solidified Ni-based superalloy. J. Manuf. Process. **30**, 208-216 (2017).

[25] R.K. Saha, T.I. Khan, Effect of bonding variables on TLP bonding of oxide dispersion strengthened superalloy. J. Mater. Sci. **42**, 9187-9193 (2007).

[26] J. Cho, F. Dong, L. Yin, D. Shaddock, Effects of The Interlayer Thickness and Alloying on The Reliability of Transient Liquid Phase (TLP) Bonding. In: 2018 IEEE 68th Electron. Compon. Technol. Conf. ECTC, IEEE, pp. 551-556 (2018).

[27] U.K. Tarai, S. Pal, P.S. Robi, The effect of post-bond solution treatment and double aging on the microstructural evolution and mechanical properties of TLP-bonded IN718 joint. Arch. Civ. Mech. Eng. **23**, 110 (2023).

[28] U.K. Tarai, S. Pal, P.S. Robi, Kinetics of isothermal solidification during transient liquid phase bonding of Inconel 718 superalloy by differential scanning calorimetry. Proc. Inst. Mech. Eng. Part J. Mater. Des. Appl. (2023).
DOI: https://doi.org/14644207231218113

[29] N. Sheng, X. Hu, J. Liu, T. Jin, X. Sun, Z. Hu, M 3 B 2 and M 5 B 3 formation in diffusion-affected zone during transient liquid phase bonding single-crystal superalloys. Metall. Mater. Trans. A **46**, 1670-1677 (2015).

[30] M. Kapoor, Ö.N. Doğan, C.S. Carney, R.V. Saranam, P. McNeff, B.K. Paul, Transient-liquid-phase bonding of H230 Ni-based alloy using Ni-P interlayer: Microstructure and mechanical properties. Metall. Mater. Trans. A **48**, 3343-3356 (2017).

[31] B. Zhang, G. Sheng, Y. Jiao, Z. Gao, X. Gong, H. Fan, J. Zhong, Precipitation and evolution of boride in diffusion affected zone of TLP joint of Mar-M247 superalloy. J. Alloys Compd. **695**, 3202-3210 (2017).

[32] U.K. Tarai, S. Pal, P.S. Robi, Reduction of ASZ size and enhancement of mechanical properties of TLP bonded IN718 joint using post bond heat treatment process. Int. J. Adv. Manuf. Technol. **129**, 1425-1442 (2023).

[33] W. Reeks, H. Davies, S. Marchisio, A review: Interlayer joining of nickel base alloys. J. Adv. Join. Process. **2**, 100030 (2020).

[34] Y. Zhang, Y. Zhong, Y. Cheng, N. He, L. He, Z. Gao, X. Gong, C. Chen, H. Ye, Microstructural evolution and micro-mechanical properties of non-isothermal solidified zone in TLP bonded Ni-based superalloy joints. J. Mater. Sci. Technol. **185**, 9-22 (2024).